VII. NUCLEAR MAGNETIC RESONANCE AND HYPERFINE STRUCTURE

Prof. F. Bitter
Prof. L. C. Bradley III
Prof. J. S. Waugh
Dr. H. H. Stroke
Dr. J. F. Waymouth
B. B. Aubrey
M. Ciftan
F. W. Dobbs

H. R. Hirsch
R. J. Hull
R. H. Kohler
R. F. Lacey
Mrs. Ilana Levitan
K. K. Li
J. H. Loehlin

A. T. Maksymowicz
I. G. McWilliams
E. C. Penski
G. H. Price
W. W. Smith
C. V. Stager
W. T. Walter
S. T. Wray, Jr.

A. NUCLEAR MAGNETIC RESONANCE

1. NUCLEAR SPIN INTERACTIONS IN MOLECULES

Most analyses of high-resolution nuclear resonance spectra have proceeded by diagonalizing the proper spin Hamiltonian (1), starting with the product representation and taking advantage of any permutation symmetry of the Hamiltonian to form suitable linear combinations of the product functions (2). When the degree of permutation symmetry is high, it may be advantageous to adopt a different approach. Imagine that the set of spins is divided into groups κ, λ, μ, ... in such a way that the Hamiltonian is invariant to permutations of nuclei within a group. Denoting the chemical shifts by δ, and the spin-spin coupling constants by A, we can write the Hamiltonian as

$$-\mathcal{H}/h = \nu_o J_z - \nu_o \delta_\kappa K_z - \nu_o \delta_\lambda L_z - \ldots + A_{\kappa\lambda}\vec{K} \cdot \vec{L} + \ldots$$

where $\vec{K}$ is the total spin angular momentum of group κ, ..., and J is the total angular momentum of the system. Since $\mathcal{H}$ commutes with K^2, L^2, ..., J_z — and J_x commutes with all but the last of these — the group moments behave, to all intents and purposes, like nuclei of permanent spin k, ℓ, ... If a representation that is diagonal in these quantities is used, the spectrum can be calculated for each k, ℓ, ... consistent with the composition of the groups, and the spectra thus obtained can be superposed, each according to the proper weighting factor N(k):

$$N(k) = \begin{pmatrix} n \\ \frac{n}{2} - k \end{pmatrix} - \begin{pmatrix} n \\ \frac{n}{2} - k - 1 \end{pmatrix}$$

where n is the number of spin $-1/2$ nuclei in group κ.

If there are only two spin groups, the effective Hamiltonian can be written

$$H' = K_z + a\vec{K} \cdot \vec{L}$$

where $a = -A_{\kappa\lambda}/(\nu_o \delta_\kappa)$, with $\delta_\lambda = 0$. In the representation described by K, L, J, J_z, the matrix elements (3) are:

$$(k, \ell, j, m \,|\, K_z \,|\, k, \ell, j, m) = \left[\frac{k(k+1) - \ell(\ell+1) + j(j+1)}{2j(j+1)} \right] m$$

$$(k, \ell, j, m \,|\, K_z \,|\, k, \ell, j-1, m) = (k, \ell, j-1, m \,|\, K_z \,|\, k, \ell, j, m)$$

$$= \left[\frac{(j-k+\ell)(j+k-\ell)(k+\ell+j+1)(k+\ell-j+1)(j^2-m^2)}{4j^2(2j-1)(2j+1)} \right]^{1/2}$$

$$(k, \ell, j, m \,|\, \vec{K} \cdot \vec{L} \,|\, k, \ell, j, m) = \frac{1}{2} \left[j(j+1) - k(k+1) - \ell(\ell+1) \right]$$

The eigenvalues follow from these elements, and the intensities can be found by writing the matrix of J_x in the same representation and applying to it the same unitary transformation that diagonalizes H'.

This method has been applied to the analysis of the spectrum of isobutane, in which one group consists of a single spin $(k = 1/2)$, and the other of nine spins $(\ell = 1/2, \ldots, 9/2)$. The product representation is not suitable for handling the secular equation of dimension 1024 that results, but the problem is very easily handled in the (k, ℓ, j, m) representation. The complex spectrum is found to be consistent with the parameters $\delta_k = -0.85 \times 10^{-6}$ and $A_{\kappa\lambda} = 6.8$ cps. A complete description of this work has been submitted to the Journal of Chemical Physics.

F. W. Dobbs, J. S. Waugh

References

1. J. S. Waugh, Nuclear spin interaction in molecules, Quarterly Progress Report, No. 52, Research Laboratory of Electronics, M.I.T., Jan. 15, 1959, p. 30.

2. H. M. McConnell, A. McLean, and C. A. Reilly, J. Chem. Phys. **23**, 1152 (1955).

3. E. U. Condon and G. H. Shortley, The Theory of Atomic Spectra (Cambridge University Press, New York, 1951), pp. 59 ff.

2. MOLECULAR MOTION IN SOLIDS

Molecular theory predicts that essentially free internal rotation should occur about the metal-cyclopentadienyl bond in ferrocene-like molecules. Nuclear resonance studies of ferrocene (1) itself have not been able to settle this matter experimentally because of the impossibility of distinguishing internal from over-all rotation of the molecule. We have looked at the linewidth behavior of bis-(cyclopentadienylmolybdenum tricarbonyl) (2), in which the latter process is certainly not possible because of molecular asymmetry.

A proton resonance linewidth transition is found in the neighborhood of 100° K, which makes it possible to set an upper limit of approximately 4 kcal/mole on the internal barrier. This value is entirely consistent with the predictions of valence theory.

J. H. Loehlin, J. S. Waugh

References

1. C. H. Holm and J. A. Ibers, J. Chem. Phys. 30, 885 (1959); cf. references therein.

2. F. C. Wilson and D. P. Shoemaker, J. Chem. Phys. 27, 809 (1957).

B. DEPENDENCE OF HYPERFINE-STRUCTURE ANOMALIES FOR $S_{1/2}$ ELECTRONS ON THE NUCLEAR CHARGE DISTRIBUTION

The evaluation of hyperfine-structure anomalies [Bohr-Weisskopf effect (1,2)] depends on the nuclear charge distribution. This dependence enters through the coefficients b; these, in turn, determine the fractional reductions κ_i of the spin and orbital parts of the hyperfine-structure interaction which result from an extended nuclear magnetization and charge distribution. In order to see how dependent the hfs anomalies are on the nuclear charge distribution, we have calculated these coefficients for the charge distributed partly uniformly through the nuclear volume (i.e., a sphere of radius R_o), and partly over the surface.

From a series solution of the Dirac equation inside the nucleus and the appropriate boundary condition at $r = R_o$, we can write for the fractional reductions in the symmetric spin, asymmetric spin, and orbital contributions of the nuclear magnetization:

$$\kappa_S = \frac{\int_0^R fg\,dr}{\int_0^\infty fg\,dr} + \zeta\frac{\int_0^R \frac{r^3}{R^3} fg\,dr}{\int_0^\infty fg\,dr} = \sum_{n=1}^\infty (-1)^{n+1} (b_{s,2n} + \zeta b'_{s,2n})\left(\frac{R^{2n}}{R_o^{2n}}\right)$$

$$\kappa_L = \frac{\int_0^R \left(1 - \frac{r^3}{R^3}\right) fg\,dr}{\int_0^\infty fg\,dr}$$

$$= \sum_{n=1}^\infty (-1)^{n+1} b_{\ell,2n}\left(\frac{R^{2n}}{R_o^{2n}}\right)$$

ζ = Bohr angular asymmetry parameter

The symbols are those of Bohr and Weisskopf (1, 4). For the given potential, we obtain for the coefficients defined above:

$$b_{s2} = \frac{R_o \gamma}{6D} (1+z)$$

$$b_{s4} = \frac{R_o \gamma}{60D} \left[3z + \frac{4}{3} \gamma^2 (1+z)^2 (2\epsilon + 1 + z) \right]$$

$$b_{s6} = \frac{R_o \gamma^3}{1890D} (1+z) \left[3\gamma^2 (1+z)^2 (2\epsilon + 1 + z)^2 + 51\epsilon z + 38z(z+1) \right]$$

$$b'_{s2} = \frac{2}{5} b_{s2} \qquad b_{\ell 2} = \frac{3}{5} b_{s2}$$

$$b'_{s4} = \frac{4}{7} b_{s4} \qquad b_{\ell 4} = \frac{3}{7} b_{s4}$$

$$b'_{s6} = \frac{2}{3} b_{s6} \qquad b_{\ell 6} = \frac{1}{3} b_{s6}$$

where

$$D = \frac{[(2\rho - 1)!]^2 \,\,\lambdabar_c \left(\dfrac{2ZR_o}{a_o} \right)^{2(1-\rho)}}{300\rho(4\rho^2 - 1)} \cdot \left[15 - \gamma^2 \left(5 + 4z + \frac{1}{2} z^2 \right) \right]^2$$

$$R_o = 1.2 \times 10^{-13} A^{1/3} \qquad a_o = \hbar^2/me^2$$

$$\gamma = Z\alpha \qquad \lambdabar_c = \alpha a_o$$

$$\alpha = \frac{e^2}{\hbar c} \qquad \epsilon = (mcR_o)/\gamma\hbar$$

$$\rho = (1 - \gamma^2)^{1/2}$$

$z = Z'/2Z$; Z = total nuclear charge; Z' = part of the nuclear charge distributed uniformly over the nuclear volume.

Numerical values were calculated for the two extreme cases of a uniform charge distribution and a surface charge distribution. We have tabulated the coefficients as a function of Z, and have assumed that $A(Z)$ equals the "line-of-stability" value as given in Sullivan's Trilinear Chart (3). The results are given in Tables VII-1 and VII-2. Our results for the uniform charge distribution differ slightly from those of Bohr and Weisskopf as tabulated in the review article of Eisinger and Jaccarino (4), because our calculations did not neglect the term ϵ. These results

Table VII-1. b coefficients (per cent) for a uniform nuclear charge distribution.

Z	b_{s2}	b_{s4}	b_{s6}	b'_{s2}	b'_{s4}	b'_{s6}	$b_{\ell 2}$	$b_{\ell 4}$	$b_{\ell 6}$
10	.064	.006		.026	.004		.038	.003	
15	.115	.012		.046	.007		.069	.005	
20	.178	.019		.071	.011		.107	.008	
25	.258	.029		.103	.016		.155	.012	
30	.354	.041	.002	.142	.023	.001	.212	.018	
35	.472	.057	.003	.189	.033	.002	.283	.024	.001
40	.612	.078	.005	.245	.044	.003	.367	.033	.002
45	.779	.105	.008	.312	.060	.005	.468	.045	.003
50	1.004	.143	.013	.402	.082	.009	.602	.061	.004
55	1.265	.191	.020	.506	.109	.013	.759	.082	.007
60	1.467	.235	.028	.587	.134	.018	.880	.101	.009
65	1.956	.334	.044	.782	.191	.029	1.173	.143	.015
70	2.408	.438	.063	.963	.250	.042	1.445	.188	.021
75	2.936	.569	.089	1.174	.325	.059	1.761	.244	.030
80	3.657	.755	.127	1.463	.432	.085	2.194	.324	.042
85	4.227	.930	.167	1.691	.531	.112	2.536	.399	.056
90	4.940	1.158	.222	1.976	.662	.148	2.964	.496	.074
95	5.626	1.404	.284	2.250	.802	.190	3.376	.602	.095

Table VII-2. b coefficients (per cent) for a surface nuclear charge distribution.

| Z	b_{s2}	b_{s4}	b_{s6}	b'_{s2}	b'_{s4}	b'_{s6}	$b_{\ell 2}$	$b_{\ell 4}$	$b_{\ell 6}$
10	.042			.017			.025		
15	.076			.031			.046		
20	.118			.047			.071		
25	.170	.001		.068			.102		
30	.233	.002		.093	.001		.140	.001	
35	.309	.003		.123	.002		.185	.001	
40	.398	.005		.159	.003		.239	.002	
45	.503	.008		.201	.004		.302	.003	
50	.643	.012		.257	.007		.386	.005	
55	.803	.019		.321	.010		.482	.008	
60	.922	.025		.369	.014		.553	.011	
65	1.215	.039	.001	.486	.022		.729	.017	
70	1.478	.055	.001	.591	.031	.001	.887	.024	
75	1.777	.076	.002	.711	.043	.001	1.066	.032	.001
80	2.180	.105	.003	.872	.060	.002	1.308	.045	.001
85	2.476	.135	.004	.991	.077	.003	1.486	.058	.001
90	2.840	.173	.006	1.136	.099	.004	1.704	.074	.002
95	3.167	.214	.008	1.267	.122	.005	1.900	.092	.003
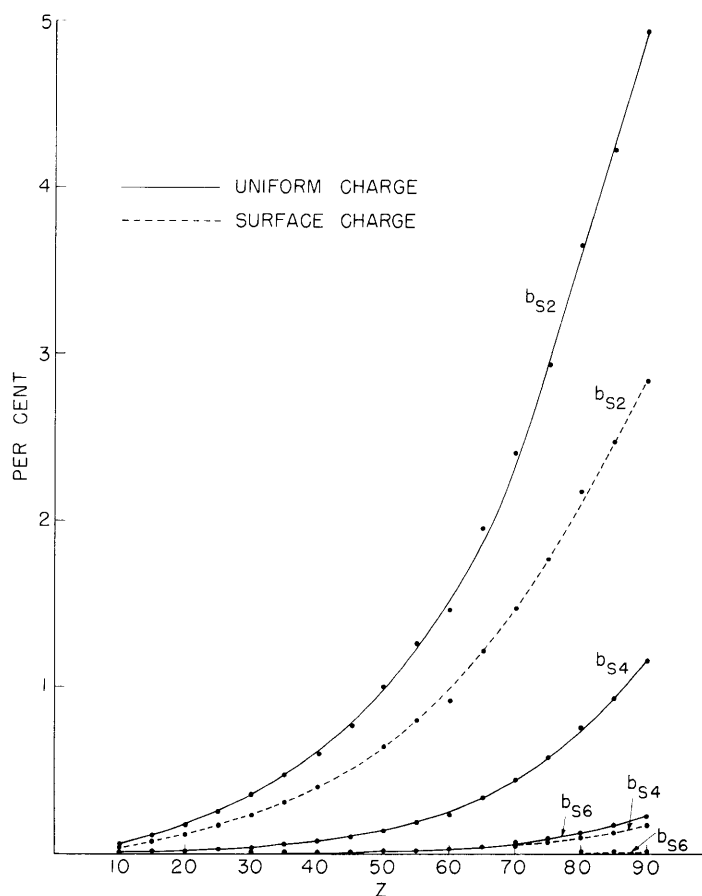
Fig. VII-1. Variation of b with atomic number for uniform
and surface charge distributions.

are also shown in Fig. VII-1. For a specific set of isotopes we could calculate
b(A), and the results would then include the Breit-Rosenthal and Crawford-Schawlow
corrections (5, 6), which are usually small. For example, for the uniform charge
distribution, the difference in b_{s2} for Z = 55 between A = 133 and A = 135 is
0.005 per cent.

It is observed from these results that the interpretation of the hfs anomalies could
be quite sensitive to the variations of nuclear charge distribution, although not to the
extent of these two extreme cases. The most favorable experimental cases would be
those for which the anomalies could be measured in three or more isotopes. The ratios
of the sizes of anomalies would then lead to information about the specific charge dis-
tribution — that is, essentially through the "scale factors" b — and the actual values
would serve as a more reliable test of the nuclear magnetization model. The charge
distribution is not expected to vary significantly from isotope to isotope, as shown by
electron-scattering data (7).

We wish to thank Miss Susan Roth, of the Joint Computing Group, M.I.T., for carrying out the numerical calculations.

H. H. Stroke

References

1. A. Bohr and V. F. Weisskopf, Phys. Rev. 77, 94 (1950).
2. A. Bohr, Phys. Rev. 81, 134 (1951), 81, 331 (1951).
3. W. H. Sullivan, Trilinear Chart of the Nuclides, Oak Ridge National Laboratory, 2d edition, 1957 (Superintendent of Documents, Washington, D.C.).
4. J. Eisinger and V. Jaccarino, Revs. Modern Phys. 30, Part I, 528 (1958).
5. J. Rosenthal and G. Breit, Phys. Rev. 41, 459 (1932).
6. M. F. Crawford and A. L. Schawlow, Phys. Rev. 76, 1310 (1949).
7. B. Hahn, R. Hofstader, and D. G. Ravenhall, Phys. Rev. 105, 1353 (1957).

C. THE ULTRAVIOLET OUTPUT OF CAPILLARY MERCURY ARC LAMPS

The work of the Magnet Laboratory has included the study of properties of atomic nuclei by their influence on the spectra of the atoms in question. One of the primary problems in the investigation of each isotope species to be studied, therefore, has been the generation of radiation for emission or absorption spectroscopy. Especially in experiments on nuclear orientation by "optical pumping," the availability of enough radiation to do the job is the key to the whole experiment.

For the majority of experiments carried out thus far, small electrodeless lamps, excited either by microwave or radiofrequency power, have proved very satisfactory. These conventionally contain a few millimeters of a buffer gas, such as argon, and a small amount of a varporizable metal whose spectrum is to be excited.

The lamps have at least one disadvantage: The amount of power conveniently obtainable at these frequencies limits the maximum radiation that can be obtained. For this reason, the study of dc and ac arcs in lamps equipped with electrodes was undertaken, so that substantially greater input power could be obtained if necessary. Mercury arcs were studied, with the production of large amounts of mercury resonance radiation, 2537 A, as the goal.

The narrowest possible linewidth for the emitted radiation was desired, so that "imprisonment" of resonance radiation was to be avoided. This dictated the use of low vapor pressures and capillary tubing of small diameter. Under these circumstances, the linewidth is determined primarily by Doppler broadening. Another goal, the achievement of thermal equilibrium between the high-temperature electrons in the arc and the excited states of mercury, was also favored by the small-diameter capillary tubing for the arc.

The thermal-equilibrium population of the excited states sets the ceiling for the amount of resonance radiation that can be obtained. The output at all times is equal to the number of excited atoms divided by the mean lifetime of the excited state. Since electrons can both "excite" ground-state atoms and "quench" excited atoms, when the electron density is sufficiently high that the frequency of exciting and quenching collisions is large in comparison with the frequency of radiating transitions, the density of excited atoms is determined by the equilibrium between the rate of excitation and the rate of quenching. If the electrons have a Maxwellian distribution of energies, this equilibrium population of excited atoms is said to be the thermal-equilibrium population and is given by

$$n_{Hg^*} = n_{Hg_o} \frac{g^*}{g_o} e^{-eV_*/kT_e}$$

where the g's are the statistical weights of the excited and ground states, respectively, and V_* is the excitation potential of the excited state.

The arc of a capillary arc tube favors the achievement of this maximum possible density of excited atoms by permitting high electron densities at moderate currents. Figure VII-2 shows the construction of the arc tubes that was used. With a capillary of this size, an electron density of approximately 10^{14} per cubic centimeter is obtained at a current of 2 amp when 2 mm argon is used as a recoil gas. The 2537 A radiation was detected by means of a scattering cell filled with mercury vapor, and a photomultiplier, as shown in Fig. VII-3. Since the scattering cell is at room temperature, its "absorption linewidth" has only the room-temperature Doppler width; therefore only the "core" or useful part of the emission line is detected.

The 2537 A output was studied as a function of rare gas pressure, mercury vapor pressure, and discharge current. Observations were made with argon, neon, helium, and no rare gas at all. With neon and helium the spectrum of the rare gas, as well as that of mercury, was obtained. With argon no such difficulty was encountered; most of the work was done with argon.

Figure VII-4 shows the curves of ultraviolet output and arc voltage drop at a fixed current as a function of argon pressure. The rare gas serves three functions: First, it retards the diffusion of excited atoms to the walls where they may give up their energy without radiation; second, it obstructs the passage of the electron drift current, thereby increasing the electron density at a given current; finally, it retards the ambipolar diffusion losses of electrons and ions to the walls, and thereby exerts a controlling influence on the electron temperature.

At low pressures, therefore, we expect the ultraviolet output to increase with increasing argon pressure, since both of the first two factors are acting to increase
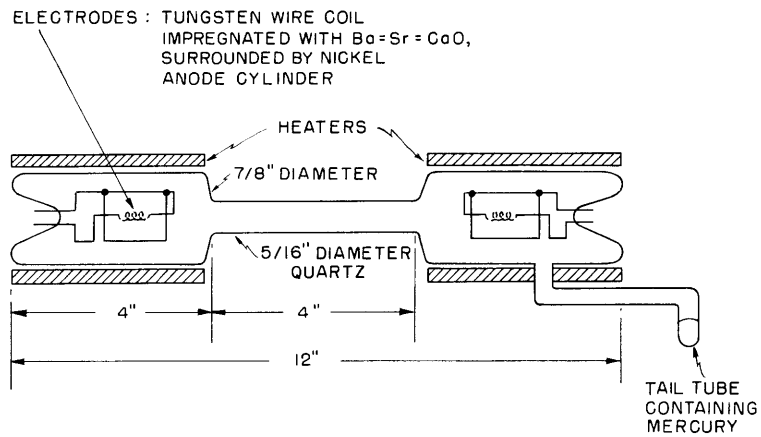
ELECTRODES : TUNGSTEN WIRE COIL
IMPREGNATED WITH Ba=Sr=CaO,
SURROUNDED BY NICKEL
ANODE CYLINDER

HEATERS

7/8" DIAMETER

5/16" DIAMETER
QUARTZ

4"

4"

12"

TAIL TUBE
CONTAINING
MERCURY

Fig. VII-2. Sketch showing construction of arc tubes.

QUARTZ SCATTERING CELL
CONTAINING MERCURY

ENTRANCE
APERTURE

ARC
TUBE

2537A
RADIATION

ULTRAVIOLET
FILTER

PHOTOMULTIPLIER
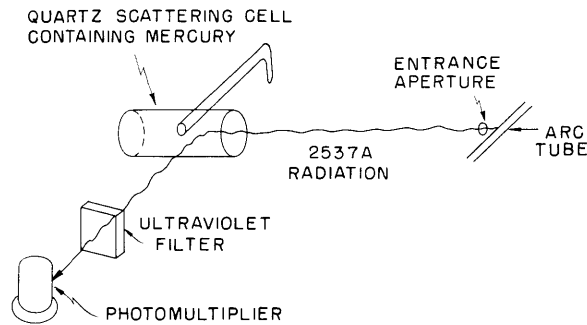
Fig. VII-3. Sketch showing light-detecting apparatus. The
whole apparatus is enclosed in a light-tight box
to reduce stray light.

ULTRAVIOLET OUTPUT

LAMP VOLTAGE DROP

LAMP VOLTAGE DROP

ULTRAVIOLET OUTPUT (ARBITRARY UNITS)

LAMP PRESSURE (MM ARGON)
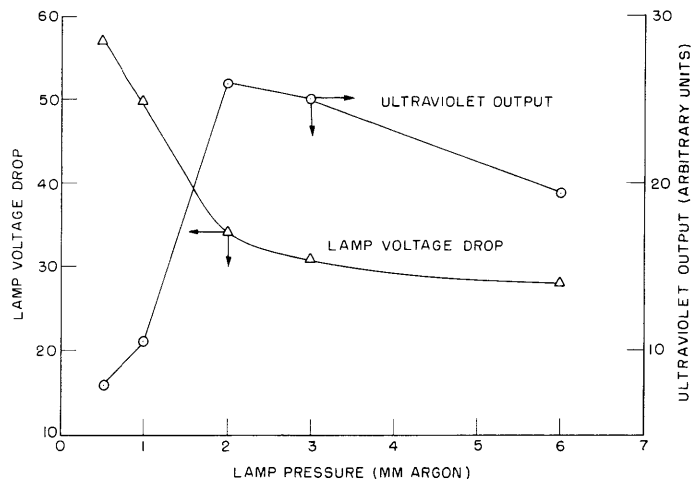
Fig. VII-4. Lamp voltage drop and ultraviolet output as a function
of argon pressure at a constant condensed-mercury
temperature, 50° C, at a constant current of 1 amp.

69

the population of excited atoms toward the equilibrium population. At the higher argon pressures, at which the thermal equilibrium of excited atoms with the hot electron gas has been approached, further increases in argon pressure decrease the electron temperature and thereby decrease the ultraviolet output. This interpretation is also borne out by the dependence of voltage drop on pressure. At low argon pressures, the voltage drop decreases sharply with increasing pressure because the increasing density of excited atoms results in more two-stage ionization and permits the arc to be maintained at a lower voltage drop. Above the pressure at which thermal equilibrium is reached, the voltage drop varies only slightly with argon pressure.

Figure VII-5 shows the dependence of ultraviolet output at 2 mm argon pressure on current and condensed-mercury temperature. The increasing output at low mercury vapor pressures is the result of the increasing number of excited atoms that radiate. The decrease in "output" at higher vapor pressures is caused by the onset of "imprisonment" of the resonance radiation and its consequent broadening of the emission line, as well as reduction of the total output. Both of these will reduce the detected signal with the arrangement of Fig. VII-3. The fact that the condensed-mercury temperature for maximum output varies with arc current indicates that the vapor density in the capillary is less than that in the condensed-mercury chamber, by an amount that depends
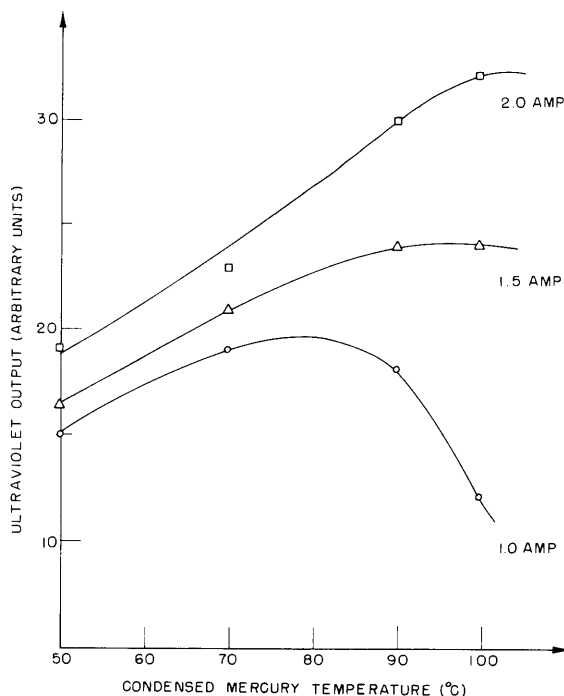

Fig. VII-5. Ultraviolet output as a function of condensed-mercury temperature, for three arc currents, at a fixed argon pressure of 2.0 mm.

70

on the arc current.

There are two reasons why this should be so: First, the temperature of the capillary is substantially higher than that of the condensed-mercury chamber. The vapor density in the capillary should be less than that in the cold chamber by the ratio of the square roots of the temperatures $(T_{chamber}/T_{capillary})^{1/2}$. Second, at these high electron densities, approximately 10 per cent of the mercury is ionized. This leads to "ionic pumping" of the mercury from the axis to the walls of the capillary. Mercury ions migrate to the walls with an ambipolar diffusion coefficient $\dfrac{\mu_i kT_e}{e}$. They are neutralized at the walls and diffuse back as neutral atoms, with diffusion coefficient $\dfrac{\mu_i kT_g}{e}$. Since the ratio of electron temperature to gas temperature is usually of the order of 30, the gradient of mercury atom density must be thirty times the ion density gradient in order for the two diffusion rates to be equal. At these high fractional ionizations, this leads to a severe depletion in mercury atom density at the axis, and hence to a lower effective vapor pressure. The higher the current, the lower the vapor density at the axis.

Figure VII-6 shows a plot of the output at optimum vapor pressure versus arc current which indicates that the desired goal of thermal equilibrium was not quite obtained. With substantially higher currents, perhaps, the output could have been increased by a factor of two.

No quantitative measurements have been made of the ultraviolet output. It has been qualitatively compared with the output from a similar small capillary tube excited by microwave power. Microwave excitation with a QK 61 magnetron at 1.25 kv produced approximately the same ultraviolet intensity in a 4-inch long capillary tube as a
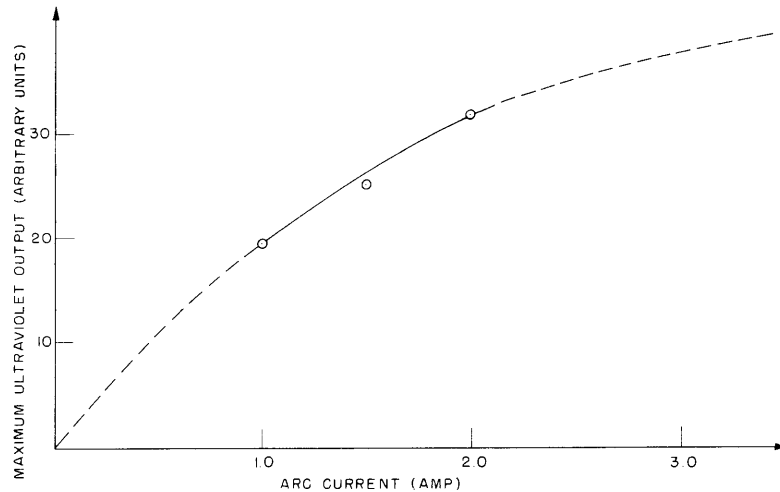

Fig. VII-6. Maximum ultraviolet output at optimum condensed-mercury temperature as a function of arc current. Argon pressure held constant at 2.0 mm.

2-amp ac arc current through a similar capillary tube.

The results obtained thus far indicate that no great improvement in ultraviolet output per unit of area is obtained by the use of lamps with electrodes. However, the ease with which a source of relatively large area can be constructed, either by mounting many capillary arcs side by side, or by "folding up" a long capillary, may well prove important in future experiments.

The experimental measurements described in this report were all made by S. W. Thompson.

J. F. Waymouth

D. CARRIER-FREE PRODUCTION OF ISOTOPES WITHOUT TRANSMUTATION

Gold targets were bombarded with 15-mev deuterons in the M.I.T. cyclotron in an attempt to knock the Au^{198} recoils from the $Au^{197}(d, p)Au^{198}$ reaction onto catcher foils placed immediately behind the targets. In this way, we hoped to separate a sufficient amount of $Au^{198}(10^{12}-10^{13}$ atoms) from the stable Au^{197} to permit a spectroscopic analysis of the Au^{198}.

Gold was used only for testing the feasibility of the recoil separation method, since Au^{198} can be obtained in other ways. Our actual interest is centered on applying this recoil separation method to produce radioisotopes, such as Tl^{204}, that cannot be easily obtained by other means. Only the difficulty of carrying out a γ-analysis for the presence of Tl^{204} prevented the use of thallium for the entire project.

Gamma-analysis of a mylar catcher from one of the gold bombardments definitely showed the presence of Au^{198} atoms on it. The estimated total yield of 10^7-10^8 atoms was far short of the $10^{12}-10^{13}$ atoms that we hoped to obtain. However, since the estimate was based on rather crude calculations, it will be necessary to attempt a spectroscopic analysis of a catcher foil from one of the bombardments to determine definitely the success or failure of this separation method. We hope that such an analysis will be carried out with one of the thallium samples.

A. T. Maksymowicz

E. HOLLOW-CATHODE DISCHARGE TUBES FOR USE WITH SMALL QUANTITIES OF SOURCE MATERIALS

A hollow-cathode discharge tube was designed to operate with very small quantities of source materials. Experiments were done with mercury, zinc, barium, and thallium.

Aluminum cathodes with cylindrical cavities of different sizes were tested. The smallest quantity of material for which a spectrum was observed with the use of a cylindrical cavity, was 0.01 mg of thallium. As soon as the discharge started, the material was presumably driven by sputtering, together with the aluminum, to the corners of the cavity where it was buried and therefore ineffective.

Following the work reported to us by D. J. Rose concerning experiments at the Bell Telephone Laboratories, cathodes with spherical cavities of different sizes were tested. The most efficient hollow cathode that operated steadily was found to be one with a spherical cavity of 1/4-inch diameter and an orifice of 1/16-inch diameter. With this type of cathode a much smaller quantity of material was sufficient for obtaining a spectrum. The smallest quantity for which a spectrum has been observed thus far is 0.01 µg of thallium (approximately 10^{14} atoms).

The buffer gases that were tried were: tank helium, pure helium, argon, and krypton. With each one of these gases a background appeared at the pressure at which the spectrum was observed. The background was least intense when krypton was used.

Ilana Levitan

F. A MAGNETIC-SCANNING EXPERIMENT

A magnetic-scanning technique for measuring isotope shift in mercury is being developed. This method employs two atomic beams to reduce the Doppler broadening (1): one for the light source, and the other for absorption of the emitted line. The emitting beam is excited by radiation from an Hg^{198} lamp, and is placed in a homogeneous magnetic field which is varied to scan the whole structure of the 2537 A mercury line. When the frequency of one of the Zeeman components of the emitted light coincides with the frequency of one of the absorption lines in the absorbing beam a decrease in the current of the detecting photomultiplier will occur. In this way, the differences in energy of the various hyperfine-structure and isotope-shift components can be accurately determined.

The apparatus was assembled but no results were obtained because the amount of light from the emitting beam was insufficient for detection with the present arrangement. In order to determine experimentally the order of magnitude of the energy of the resonance radiation that could be expected from the atomic-beam light source, measurements were made of the amount of light scattered at right angles from a cell filled with natural mercury. The tail of the cell was kept at various temperatures, ranging from –35° C to –15° C, in order that the number of mercury atoms in the cell would agree with the calculated value of 5×10^{11} that is expected in the atomic beam. Typical values for the power scattered into a solid angle of approximately 10^{-3} steradians was approximately 0.3 µwatt.

The atomic-beam apparatus that was originally designed is now being investigated to determine some of the design parameters for the beam that will ultimately be used in this experiment.

I. G. McWilliams

References

1. F. Bitter, Atomic-beam light sources, Quarterly Progress Report, Research Laboratory of Electronics, M.I.T., April 15, 1957, pp. 29-35.